Continued Development of an SI Engine Model Using Fractal Geometry

Y.W.Chin, R.D.Matthews and S.P.Nichols
ETC 7.123
The University of Texas at Austin
Austin, TX 78712
U.S.A.
T.M.Kiehne
Defense Advanced Research Project Agency

ABSTRACT

An initial study of the use of fractal geometry to model the effects of turbulence on flame propagation in a 4-stroke, homogeneous charge SI engine was previously reported (1,2). However, two physically unrealistic assumptions were made in the model formulation to allow this technique to be investigated as expeditiously as possible. Specifically, heat loss and blowby were neglected in the initial development. Nevertheless, the initial predictions of the Fractal Engine Model (FEM) showed promise that the use of fractal geometry could prove to be a valuable new tool. These two modeling assumptions have been removed and the predictions of the modified FEM are reported.

INTRODUCTION

It has been shown that flames in homogeneous charge SI engines away from the lean limit fall into the turbulent flame category of wrinkled laminar flames (e.g., Ref. 3). For this category of turbulent premixed flames, the sole effects of turbulence are to wrinkle the flame (and thereby increase the surface area of the flame) and to stretch the flame. Fractal geometry, as initially applied to model turbulent combustion by Gouldin (4), provides a tool to account for the flame wrinkling process via a relationship that states that the turbulent flame speed is a function of the ratio of the maximum-to-minimum flame wrinkling scales, of the fractal dimension, and of the effects of stretch:

$$u_T = u_L \frac{A_T}{A_L} = u_L \left(\frac{L_{max}}{L_{min}}\right)^{D_3 - 2} \quad (1)$$

where u_T is the turbulent flame speed, u_L is the stretched laminar flame speed, A_T/A_L is the fractional increase in flame surface area due to the wrinkling caused by the turbulent flow field, L_{max} and L_{min} are the maximum and minimum flame wrinkling scales, and D_3 is the fractal dimension of a rough (and/or fragmented) surface in 3-dimensional topological space, which characterizes the roughness or degree of wrinkling of the flame.

The FEM code uses a hueristic equation (5) which accounts for variable fractal dimension during the combustion process, as a function of the turbulence intensity (u') and of the unstretched laminar flame speed (S_L):

$$D_3 = 2.35 \frac{u'}{u' + S_L} + 2.0 \frac{S_L}{u' + S_L} \quad (2)$$

which has been shown to yield good agreement with experimental data for flames in engines (1,2). Variable stretch effects are also included using a model developed by Law (6):

$$u_L = S_L \left(1 - \frac{\nu}{S_L^2} K\right) \quad (3)$$

where ν is the kinematic viscosity of the unburned mixture and K is the flame stretch factor. The flame stretch factor is assumed to be composed of two additive components (7) and is modeled using:

$$K = K_E + K_S = \frac{2}{r_f}\frac{dr_f}{dt} + \sqrt{\frac{\varepsilon}{C_3^{4/3}\nu}} \quad (4)$$

where K_E is the flame stretch factor associated with flame expansion, K_S is the stretch factor associated with flame strain, ε is the rate of dissipation of turbulent kinetic energy, and C_3 relates the minimum flame wrinkling scale to the Kolmogorov length scale.

A global (zero-dimensional) turbulence model is used which is identical to that used by Poulos and Heywood (8), except that the means for determining the integral length scale, L_i, does not change after ignition in the present case. The eddy burning model uses rapid distortion theory after ignition to calculate the integral scale and turbulence intensity to account for the dilatation effect. However, because the predicted increase in turbulence intensity and decrease in length scale has not been confirmed by experiment, in the present case the length scales and turbulence intensity after ignition are calculated using the same technique as used prior to ignition. Another modification to the global turbulence model used, in comparison to the formulation presented by Poulos and Heywood, is that the adjustable constant, C_β, is determined given the turbulent kinetic energy at intake valve closing and the turbulence intensity at the time of the spark in the present formulation.

In recognition that laminar flame propagation smooths the small scale wrinkles, the minimum flame wrinkling scale was taken to be 3.55 times η, the Kolmogorov scale (thus, $C_3 = 3.55$). This estimate was based upon experimental measurements in burner-type flames (9-11) since L_{min} has not been resolved in engine experiments. Also in burner-type flames, it has been shown that the maximum flame wrinkling scale is larger than the integral length scale. In the author's opinions, L_{max} has not been resolved in engines either. Thus, 3 different assumptions were made for L_{max}: (1) $L_{max} = 2L_i$ (as suggested by the work of North aand Santavicca (12)), (2) $L_{max} = h_{gap}$ (which, in the present case, is essentially equivalent to letting $L_{max}/L_{min} = L_i/\eta$), and (3) $L_{max} = r_F$, the flame radius (the maximum possible flame wrinkling scale). These assumptions bracket the physically possible limits of the increase in flame surface area due to flame wrinkling.

Finally, although prior quasidimensional engine models assumed that the flame expands spherically, Barr and Witze (13) showed that this is not true. For the present work, a crude model to account for nonspherical flame propagation has been used which is based upon Barr and Witze's results. The flame is assumed to expand spherically away from the spark plug until the flame reaches the piston, following which the average flame area is multiplied by 1.1 to account for flame distortion. It should be noted that Barr and Witze's work accounted only for thermal interactions with the walls and not for momentum interactions with the bulk motion of the reactants.

The model predictions were compared to experimental data from an engine with an axisymmetric pancake-shaped combustion chamber (14) and there was no attempt to adjust the code to fit the experimental data (other than through "tuning" the turbulence submodel). The initial version of the FEM accurately predicted the initial rate of pressure rise independent of assumptions made about the wrinkling scales or the effects of stretch. Also, the predicted position of peak pressure was within 5 CA° of the experimental value. Further evidence that this technique is promising is that the predicted trend of the turbulent flame speed was shown to agree with experimental observations. However, the pressure profile after early flame growth was typically overpredicted. Inclusion of heat transfer and blowby in the model was expected to decrease the pressures to values closer to the experimental pressure profile, and investigation of this was the intent of the present study.

II. HEAT TRANSFER AND BLOWBY SUBMODELS

Between intake valve closure and exhaust valve opening, the First Law for the entire cylinder is:

$$\frac{dU}{d\theta} = -P\frac{dV}{d\theta} - \frac{dQ}{d\theta} - \frac{\dot{m}_B h_B}{\omega} \qquad (5)$$

where the final two terms, representing heat loss and blowby, were neglected in the initial version of the FEM but are the focus of the present study.

In the blowby term of Eqn. 5, $\dot{m}_B$ is the mass blowby rate, h_B is the enthalpy associated with the blowby, and ω is the engine rotational frequency. The crevice flow model developed by Kuo and coworkers (15), and implemented by Reitz and Kuo (16) to the same engine examined in this study, was adopted in modified form to model the blowby. Specifically, only a single ring was modeled, the pressure in the crankcase was assumed to be atmospheric, and a complete cycle simulation was not run (and thus the simulation was not iterated over several cycles to attain convergence on the ring positions). These simplifications were made to allow examination of the blowby effect on the pressure history as expeditiously as possible and refinements are planned for future work.

The heat transfer was modeled using a 2-zone (burned and unburned) application of Woschni's Nusselt number correlation with his characteristic velocity equation (17), but the composition and temperature dependent transport properties were calculated using TRANFIT (18), yielding zone-dependent convective heat transfer coefficients. Annand's equation (19), without the radiation term, was also investigated as part of a sensitivity analysis. For a 2-zone analysis, it is most convenient to refomulate the integral energy equation, which can be shown to be:

$$\omega\frac{d}{d\theta}\int_z h\,dm = \sum_j \dot{m}_{j,z} h_{j,z} + \dot{P} V_z + \dot{Q}_z \qquad (6)$$

which is applied independently to each zone and where the summation accounts for both the blowby in that zone and for the energy exchange between zones due to flame propagation.

The determination of the left hand side of Eqn. 6 requires knowledge of the mass average temperatures in the burned and unburned zones. Assuming uniform composition in each zone, the mass averaged temperature in each zone is:

$$T_{m,z} = \frac{1}{m_z}\int_z T\,dm = \frac{PV_z}{m_z R_z} \qquad (7)$$

where z=b in the burned zone and z=u in the unburned zone. The boundary layer temperature profile was modeled using a wall function:

$$\frac{T - T_w}{T_{\infty,z} - T_w} = \left(\frac{y}{\delta}\right)^{1/n} \qquad (8)$$

where δ is the boundary layer thickness, T_w is the wall temperature, and $T_{\infty,z}$ is the adiabatic core temperature of the zone of interest. The value of n=3, as suggested by Lucht and Dunn-Rankin (20), was used, although the traditional value of n=7 could easily be explored in the future. The total mass in each zone is provided by the fractal burning model, but the apportionment between core and boundary layer mass must also be known. The boundary layer mass for each zone is:

$$m_{BL,z} = \int_{BL,z}\rho\,dV = \int_{BL,z}\frac{PV}{RT}\,d\left(\frac{y}{\delta}\right) = \frac{PV_{BL,z}}{R_z T_{\infty,z}}(1+f_{BL,z}) \qquad (9)$$

where:

$$f_{BL,z} \equiv \sum_{r=1}^{\infty}\frac{\Gamma(n+1)\,\Gamma(r+1)}{\Gamma(n+r+1)}\left(1-\frac{T_w}{T_{\infty,z}}\right)^r \qquad (10)$$

Substituting Eqn. 8 into 9 and combining with the Ideal Gas Equation of State yields:

$$\frac{m_{BL,z}}{m_z} = \left(1+\frac{1}{f_{BL,z}}\right)\left(1-\frac{T_{m,z}}{T_{\infty,z}}\right) \qquad (11a)$$

and

$$\frac{m_{\infty,z}}{m_z} = 1 - \left(1+\frac{1}{f_{BL,z}}\right)\left(1-\frac{T_{m,z}}{T_{\infty,z}}\right) \qquad (11b)$$

The temperature and composition dependent properties in each zone are calculated using a Taylor series expansion at the mass average temperature. For example, the enthalpy is:

$$h(T) = h(T_m) + \frac{\partial h(T_m)}{\partial T}(T-T_m) + \frac{1}{2}\frac{\partial^2 h(T_m)}{\partial T^2}(T-T_m)^2 + \ldots$$
$$\approx h^0(T_m) + h'(T_m)(T-T_m) + \frac{1}{2}h''(T_m)(T-T_m)^2 \qquad (12)$$

where the pressure dependency of the enthalpy in the burned zone (via the equilibrium composition calculations) has been omitted from the nomenclature for the sake of brevity. The mass average enthalpy in each zone can now be determined using Eqns. 11 and 12:

$$h_{m,z}(T_{m,z}, T_{\infty,z}, T_w) = \frac{1}{m_z}\int_z h(T)\,dm \qquad (13)$$
$$= h^0(T_{m,z}) - \frac{1}{2}h''(T_{m,z})(T-T_{m,z})\left\{\frac{1}{n+1}\frac{1}{f_{BL,z}}(T_{\infty,z}-T_w) - T_{m,z}\right\}$$

The core temperature in both zones is needed for use in Eqns. 8-13 and the core temperature in the unburned zone must also be determined to allow calculation of S_L, which appears in Eqns. 2 and 3. These core temperatures are found by applying Equation 6 to the core region of each zone, omitting the heat transfer and blowby terms.

RESULTS

The model predictions are discussed in the following subsections. The effects of heat loss on the pressure history are discussed first, followed by an analysis of heat loss models and then by a discussion of the effects of blowby. Where possible, the model predictions are compared to experimental data from Groff and coworkers (14) and Alkidas and Myers (21) for the axisymmetric, pancake-shaped combustion chamber specified in Table I.

Effects of Heat Loss

Figure 1 shows the predicted pressure profiles with and without heat loss but neglecting blowby. Predictions are shown for the three different assumptions regarding the flame wrinkling scales discussed previously. Woschni's equation was used for the three cases for which heat transfer was included in the model formulation. In all three cases, the inclusion of heat transfer decreases the error in the predicted pressure at the time of ignition from a 4.4% overprediction to a 2.6% overprediction

For the assumption that the maximum flame wrinkling scale is equal to the flame radius, inclusion of heat transfer: (1) improves the prediction of the maximum pressure from a 26.6% overprediction to a 21.8% overprediction, (2) delays the predicted position of peak pressure by 1 CA°, from 5 CA° to 4 CA° before the actual position of peak pressure, (3) decreases the maximum error in the predicted pressure from a 32.8% overprediction (at the position of the predicted maximum pressure) to a 26.1% overprediction (1 CA° after the position of the predicted maximum pressure), and (4) improves the range over which the predicted early pressure rise is accurate within 10 % of the experimental value from 15 CA° after ignition to 20 CA° after ignition.

For the assumption that the maximum flame wrinkling scale is equal to the instantaneous gap, inclusion of heat transfer: (1) improves the prediction of the maximum pressure from an 11.9% overprediction to a 5.3% overprediction, (2) delays the predicted position of peak pressure by 1 CA°, from 1 CA° to 2 CA° after the actual position of peak pressure, and (3) decreases the maximum error in the predicted pressure from a 12.2% overprediction (at the position of the predicted maximum pressure)to an 8.1% overprediction (26 CA° before the position of the predicted maximum pressure). Without heat loss, the rate of early pressure rise is predicted within 10% of the experimental data for 15 CA° following ignition. Inclusion of heat transfer results in predicted pressures that are within 8.1% of the experimental data throughout the compression-combustion-expansion process.

For the assumption that the maximum flame wrinkling scale is equal to twice the integral length scale, inclusion of heat transfer: (1) worsens the prediction of the maximum pressure from a 0.9% overprediction to a 6.3% underprediction, (2) delays the predicted position of peak pressure by 2 CA°, from 4 CA° to 6 CA° after the actual position of peak pressure, and (3) worsens the maximum error in the predicted pressure from a 10.5% underprediction (9 CA° before the position of the predicted maximum pressure) to a 16.6% underprediction (11 CA° before the position of the predicted maximum pressure).

Analysis of Heat Loss Models

Figure 2 compares the heat flux predictions using Woschni's equation with those resulting from use of Annand's equation. Predictions are shown for both the burned zone and the unburned zone. In all cases, the maximum flame wrinkling scale was assumed to be equal to the instantaneous gap. This baseline was chosen simply because it provides a more accurate prediction of the pressure history and it has been shown (22) that the heat flux is dominated by the rate of pressure rise (in comparison to effects due to swirl and/or tumble) unless the engine is operating far from MBT timing (23).

Both models predict peak heat fluxes of the order of 2 MW/m^2, if α is set equal to 0.6 in Annand's equation. This peak surface-averaged value agrees with the spatially-resolved measurements of Alkidas and Myers (21), which were taken using the engine being modeled in this study. It is noteworthy that these spatially-resolved measurements showed little variation with position, except for one location, indicating that the predicted spatially-averaged peak fluxes agree well with experimental measurements for this engine. However, the Annand correlation predicts a very high flux in the burned zone during early flame growth and a relatively high rate of increase of heat flux in the unburned zone. It is difficult to make a direct comparison with the data of Alkidas and Myers since the FEM code predicts the heat flux averaged over the areas in each zone, while the data are for a fixed position which starts in the unburned zone and ends in the burned zone. However, the models predict that the flux in the burned zone never exceeds 950 kW/m^2. Thus, assumption that 1 MW/m^2 is a value which represents the burned zone allows comparison of the predictions with the data. The experimental data show an increase of heat flux from 1 MW/m^2 to the peak value over a crankangle interval of about 10-15 CA°. Annand's equation predicts an increase in flux in the burned zone from 1 MW/m^2 to the peak over a crankangle interval of about 31 CA° while Woschni's equation predicts this rise in heat flux to occur over a crankangle range of about 13 CA°. Further, Borman and Nishiwaki (24) note that, for a homogeneous charge spark ignition engine, typically 10% of the fuel energy is lost to heat transfer during the combustion process and 15% is lost to heat transfer during the combined combustion and expansion processes. The current formulation of use of Woschni's relations predicts values of about 5% during combustion and 14% for the combustion-expansion process, while Annand's equation predicts values of about 13% and 34%, respectively. For these reasons, it is believed that Woschni's equation (with zone-dependent heat transfer coefficients) is more physically realistic, at least for this engine under this set of operating conditions.

Figure 3 illustrates the effect of the heat flux model on the cylinder pressure history. Both models predict essentially the same early rate of pressure rise because the heat loss is dominated by the high temperature gradient in the burned zone, but the surface area in the burned zone is small during early flame growth. However, because of the higher predictions of heat flux in both the burned and unburned zones by the Annand equation, the cylinder pressure is underpredicted following early flame growth, the predicted peak pressure is too low, and the position of peak pressure is delayed.

Effects of Blowby

As noted previously, the experimental engine was oversimplified in the model via assumption of only a single ring. Further, initial calculations were performed assuming that the sole effect was loss of mass from the combustion chamber via blowby from the cylinder to the crankcase. The blowby mass was calculated to be about 1 % of the cylinder mass, in agreement with the more detailed calculations of Reitz and Kuo (16), indicating

that little of the cylinder mass that escapes past the top ring re-enters the cylinder during expansion, a conclusion that might be expected from the pressure histories for the regions between the rings presented by Reitz and Kuo. However, for this initial analysis, it was found that there was almost no effect on the predicted pressure history, in contrast to the 6-8% decrease in pressure predicted by Reitz and Kuo. Therefore, the top-land crevice volume and the volume behind the top ring were then accounted for in the model.

The resulting predictions are shown in Fig. 4. Again, the basecase was for the assumption that the maximum flame wrinkling scale is equal to the instantaneous gap, because this assumption yields the most accurate pressure history and the crevice-filling/blowby process is dominated by the effects of cylinder pressure. It was assumed that the mass re-entering the combustion chamber from the crevice region was burned instantaneously. Inclusion of the crevice-filling process resulted in a decrease of the peak cylinder pressure of 3.2% and advancement of the position of peak pressure by 1 CA°. Although this does not agree precisely with the predictions of the more detailed analysis of Reitz and Kuo, it is of the correct order of magnitude and is surprisingly good considering the simplifications made in the formulation of the crevice flow submodel.

SUMMARY AND CONCLUSIONS

The predictions of the current version of the Fractal Engine Model are presented in Fig. 5. The simplified crevice-flow submodel is included and Woschni's equation is used to model the heat loss. Results for all three possible assumptions regarding the maximum flame wrinkling scale are shown because the author's do not believe that sufficient experimental evidence currently exists to identify which most accurately represents the physics of the flame wrinkling process in an engine. Obviously, the assumption that $L_{max} = h_{gap}$ (which, for this case, is essentially equivalent to letting $L_{max}/L_{min} = L_t/\eta$) provides the most accurate predictions of the cylinder pressure history (within 7% throughout the entire process, with an error of the predicted peak pressure of only 1.9% and a prediction of the position of peak pressure that is within 1 CA° of the experimental value).

The following conclusions may be drawn from the present investigation:

1) The 2-zone formulation of Woschni's equation, as developed using zone-dependent heat transfer coefficients, appears to represent the heat flux in this particular engine well.
2) A simplifed crevice-flow model yields predictions that are close to those provided by a more detailed analysis. The blowby mass is predicted to have little effect on the cylinder pressure history, but the mass trapped in the crevice volume was found to have an effect of the order of that found by a more detailed prior analysis (16).
3) Inclusion of heat loss and blowby in the Fractal Engine Model improves the predictions of peak cylinder pressure, position of peak cylinder pressure, and cylinder pressure history, except in the case of the assumption that the maximum flame wrinkling scale is twice the integral length scale.
4) Most importantly, it has been shown that use of fractal geometry to model turbulent combustion in SI engines is an important new engineering tool. However, many unresolved issues regarding the fractal characteristics of flames in engines remain unanswered and merit experimental investigation.

ACKNOWLEDGEMENTS

This material is based upon work supported by the National Science Foundation under Grant No. CBT-8807169. The Government has certain rights in this material. This material is also based in part upon work supported by the Governor's Energy Management Center - State of Texas Energy Research in Applications Program under Contract No. 5127. Additional funding for this investigation was provided by Cray Research, Inc., and the research was conducted in the General Motors Foundation Combustion Sciences and Automotive Research Laboratories on the campus of the University of Texas. Any opinions, findings, and conclusions and recommendations expressed in this material are those of the authors and do not necessarily reflect the views of the National Science Foundation, of Cray Research, or of the General Motors Corporation.

REFERENCE LIST

1. Chin, Y-W., Matthews, R.D., Nichols, S.P., and Kiehne, T.M., "Use of fractal geometry to model turbulent combustion in a quasi-dimensional engine code," Western States Section of the Combustion Institute Paper WSS/CI 89-27, March, 1989.
2. Chin, Y-W., Matthews, R.D., Nichols, S.P., and Kiehne, T.M., "Use of fractal geometry to model turbulent combustion in SI engines," submitted to Comb. Sci. & Tech., 1990.
3. Keck, J.C., Heywood, J.B., and Noske, G., "Early flame development and burning rates in spark ignition engines and their cyclic variability," SAE Technical Paper 870164, 1987.
4. Gouldin, F.C., " An application of fractals to modeling premixed turbulent flames," *Combustion & Flame* **68**(3):249-266, 1987.
5. Liou, D., North, G.L., and Santavicca, D.A., "A fractal model of turbulent flame kernel growth," SAE Technical Paper 900024, 1990.
6. Law, C.K., "Dynamics of stretched flames," 22nd Symposium (International) on Combustion, The Combustion Institute, Pittsburgh, pp. 1381-1402, 1988.
7. Chung, S.H., and Law, C.K., "An invariant derivation of flame stretch," *Combustion & Flame* **55**: 123-125, 1984.
8. Poulos, S.G., and Heywood, J.B., " The effect of chamber shape on spark ignition engine combustion," SAE Technical Paper 830334, 1983.
9. Gokalp, I., "An evaluation of the Klimov-Williams criterion," *Combustion and Flame* **67**: 111-119, 1987.
10. Gouldin, F.C., Hilton, S.M., and Lamb, T., "Experimental evaluation of the fractal geometry of flamelets," 22nd Symposium (International) on Combustion, The Combustion Institute, Pittsburgh, pp. 541-550, 1988.
11. Murayama, M., and Takeno, T., "Fractal-like character of flamelets in turbulent premixed combustion," 22nd Symposium (International) on Combustion, the Combustion Institute, Pittsburgh, pp. 551-559, 1988.
12. North, G.L., and Santavicca, D.A., "The fractal nature of premixed turbulent flames," accepted for publication in Combustion Science & Technology, 1990.
13. Barr, P., and Witze, P.O., "Some limitations to the spherical flame assumptions used in phenomenological engine models," SAE Technical Paper 880129, 1988.
14. Groff, E.G., Alkidas, A.C., and Myers, J.P., General Motors Research Laboratories Report No. 3577, 1981.

15. Kuo, T-W., Sellnau, M.C., Theobald, M.A., and Jones, J.D., "Calculation of flow in the piston-cylinder-ring crevices of a homogeneous-charge engine and comparison with experiment," SAE Technical Paper 890838, 1989.
16. Reitz, R.D., and Kuo, T-W., "Modeling of HC emissions due to crevice flows in premixed-charge engines," SAE Technical Paper 892085, 1989.
17. Woschni, G., "A universally applicable equation for the instantaneous heat transfer coefficient in the internal combustion engine," SAE Technical Paper 670931, 1967.
18. Kee, R.J., Warnatz, J., and Miller, J.A., "A FORTRAN computer code package for the evaluation of gas-phase viscosities, conductivities, and diffusion coefficients," Sandia National Laboratories Report SAND83-8209, 1983.
19. Annand, W.J.D., "Heat transfer in the cylinders of reciprocating internal combustion engines," *Proc. Inst. Mech. Engrs.* **177** (36):973-990, 1963.
20. Lucht, R.P., and Dunn-Rankin, D., "Cars measurements of thermal boundary layer development in an internal combustion engine," Western States Section of the Combustion Institute Paper WSS/CI 88-56, March, 1988.
21. Alkidas, A.C., and Meyers, J.P., "Transient heat-flux measurements in the combustion chamber of a spark-ignition engine," Trans. ASME, *Journal of Heat Transfer* **104**: 62-67, 1982.
22. Alkidas, A.C., personal communication, based upon GM research to be published, 1990.
23. Alkidas, A.C., Puzinauskas, P.V., and Peterson, R.C., "Combustion and heat transfer studies in a spark ignited multivalve engine," SAE Technical Paper 900353, 1990.
24. Borman, G., and Nishiwaki, K., " Internal-combustion engine heat transfer," *Progress in Energy and Combustion Science* **13**:1-46, 1987.
25. Abraham, J., Bracco, F.V., and Reitz, R.D., "Comparisons of computed and measured premixed charge engine combustion," *Combustion and Flame* **60**:309-322, 1985.

Table I. Engine specifications (14).

Configuration:	axisymmetric pancake
Compression ratio:	8.56
Bore:	105.0 mm
Stroke:	95.25 mm
Connecting rod length:	158.0 mm
Clearance gap at TDC:	12.6 mm
Intake valve closing:	243 °ATDC
Exhaust valve opening:	103 °ATDC
Ignition timing:	27 °BTDC
Engine speed:	1500 rpm
Volumetric efficiency:	40.2%
Turbulent k. e. at intake valve closing*:	22.1 m^2/s^2
Turbulent int. at time of spark:	3.41 cm/s
Spark plug gap*:	1.0 mm
Mixture:	propane/air, $\phi = 0.869$
Residual fraction:	12 % by mass
Wall temperature**:	420 K
Ring end gap area**:	0.161 mm^2
Top ring width**:	3.55 mm
Top-land crevice volume**:	633.3 mm^3
Volume behind top ring**:	472.0 mm^3

* - From Ref. 25; ** - From Ref. 16

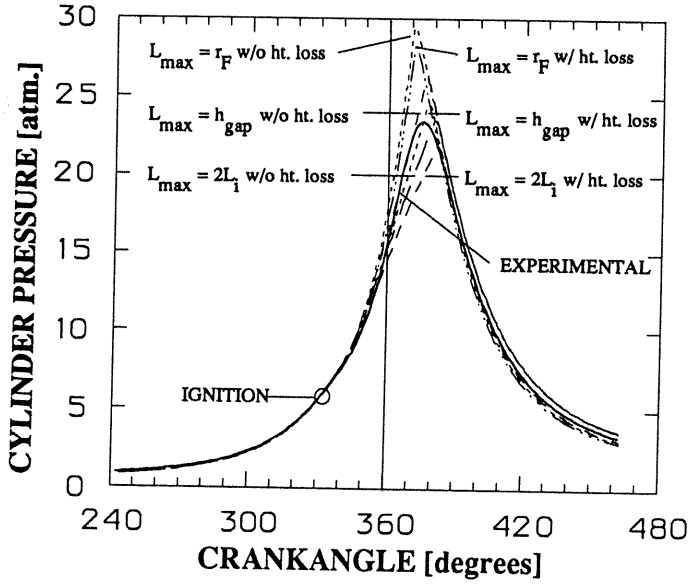

Fig. 1. Effect of heat transfer model without crevice-flow model on the predicted pressure histories for three assumptions about the maximum flame wrinkling scale.

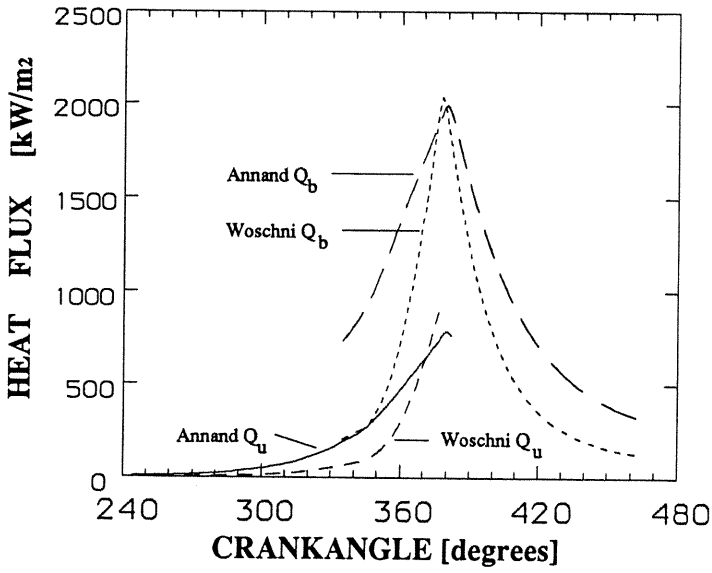

Fig. 2. Effect of choice of heat transfer model on predicted heat fluxes (surface-average in each zone).

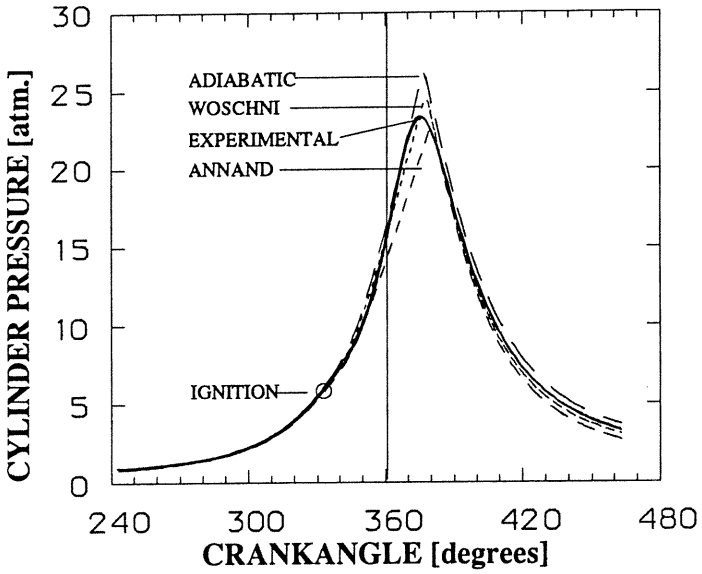

Fig. 3. Effect of choice of heat transfer model on the predicted pressure profile (L_{max} assumed to equal h_{gap}).

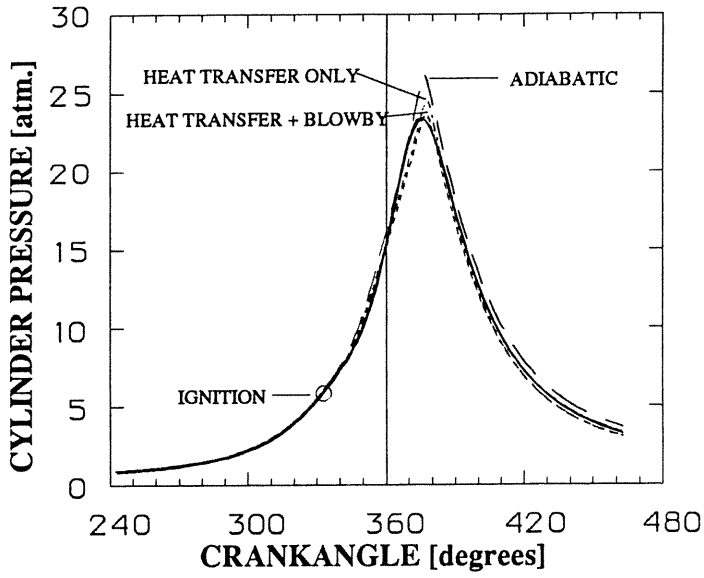

Fig. 4. Effects on the predicted pressure history using only the 2-zone Woschni heat transfer and using the heat transfer model plus a model for crevice-flow (L_{max} assumed to equal h_{gap}).

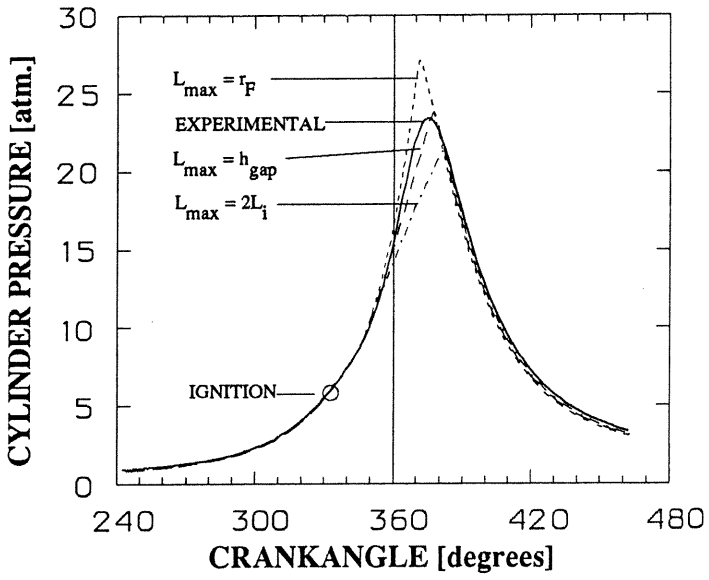

Fig. 5. Predicted pressure profiles of the FEM code including heat transfer and crevice-flow for three assumptions about the maximum flame wrinkling scale.